Influence of Molecular Geometry, Exchange-Correlation Functional, and Solvent Effects in the Modeling of Vertical Excitation Energies in Phthalocyanines Using Time-Dependent Density Functional Theory (TDDFT) and Polarized Continuum Model TDDFT Methods: Can Modern Computational Chemistry Methods Explain Experimental Controversies?

Victor N. Nemykin,[*,†] **Ryan G. Hadt,**[†] **Rodion V. Belosludov,**[*,‡] **Hiroshi Mizuseki,**[‡] **and Yoshiyuki Kawazoe**[‡]

Department of Chemistry and Biochemistry, University of Minnesota Duluth, Duluth, Minnesota 55812, and Institute for Materials Research, Tohoku University, Sendai 980-8577, Japan

Received: July 27, 2007; In Final Form: September 11, 2007

A time-dependent density functional theory (TDDFT) approach coupled with 14 different exchange-correlation functionals was used for the prediction of vertical excitation energies in zinc phthalocyanine (PcZn). In general, the TDDFT approach provides a more accurate description of both visible and ultraviolet regions of the UV–vis and magnetic circular dichroism (MCD) spectra of PcZn in comparison to the more popular semiempirical ZINDO/S and PM3 methods. It was found that the calculated vertical excitation energies of PcZn correlate with the amount of Hartree–Fock exchange involved in the exchange-correlation functional. The correlation was explained on the basis of the calculated difference in energy between occupied and unoccupied molecular orbitals. The influence of PcZn geometry, optimized using different exchange-correlation functionals, on the calculated vertical excitation energies in PcZn was found to be relatively small. The influence of solvents on the calculated vertical excitation energies in PcZn was considered for the first time using a polarized continuum model TDDFT (PCM-TDDFT) method and was found to be relatively small in excellent agreement with the experimental data. For all tested TDDFT and PCM-TDDFT cases, an assignment of the Q-band as an almost pure a_{1u} (HOMO) $\rightarrow$ e_g (LUMO) transition, initially suggested by Gouterman, was confirmed. Pure exchange-correlation functionals indicate the presence of six ^1E_u states in the B-band region of the UV–vis spectrum of PcZn, while hybrid exchange-correlation functionals predict only five ^1E_u states for the same energy envelope. The first two symmetry-forbidden n $\rightarrow$ π^* transitions were predicted in the Q_{0-2} region and in the low-energy tail of the B-band, while the first two symmetry-allowed n $\rightarrow$ π^* transitions were found within the B-band energy envelope when pure exchange-correlation functionals were used for TDDFT calculations. The presence of a symmetry-forbidden but vibronically allowed n $\rightarrow$ π^* transition in the Q_{0-2} spectral envelope explains the long-time controversy between the experimentally observed low-intensity transition in the Q_{0-2} region and previous semiempirical and TDDFT calculations, which were unable to predict any electronic transitions in this area. To prove the conceptual possibility of the presence of several degenerate ^1E_u states in the B-band region of PcZn, room-temperature UV–vis and MCD spectra of zinc tetra-*tert*-butylphthalocyanine (Pc'Zn) in non-coordinating solvents were recorded and analyzed using band deconvolution analysis. It was found that the B-band region of the UV–vis and MCD spectra of Pc'Zn can be easily deconvoluted using six MCD Faraday *A*-terms and two MCD Faraday *B*-terms with energies close to those predicted by TDDFT calculations for ^1E_u and $^1A_{2u}$ excited states, respectively. Such a good agreement between theory and experiment clearly indicates the possibility of employing a TDDFT approach for the accurate prediction of vertical excitation energies in phthalocyanines within a large energy range.

Introduction

Phthalocyanines (Pc's) belong to an important class of macrocyclic compounds because of their wide range of applications that vary from their traditional use as blue or green dyes[1] to new applications in catalysis,[2] photodynamic therapy of cancer,[3] nanotechnology,[4] and nonlinear optics.[5] The majority of these applications exploit the unique optical properties of Pc's, and thus a variety of spectroscopic techniques such as UV–vis spectroscopy, magnetic circular dichroism (MCD), and fluorescent as well as time-resolved fluorescent spectroscopy were used in the characterization of the excited states of Pc's and their analogues. Among different Pc's and their analogues, PcZn is often used as a good starting model for the understanding of phthalocyanine-based excited-state properties because of the presence of a closed-shell d^{10} configuration of the central atom (which simplifies UV–vis and MCD spectra due to the absence of additional metal-to-ligand charge-transfer and ligand-to-metal charge-transfer transitions) and the high symmetry (D_{4h}) of the complex.[6]

The first UV–vis data on transition-metal phthalocyanines (PcM) were reported by Linstead and co-workers more than 60 years ago.[7] Since then, spectra of different phthalocyanines,

* Authors to whom correspondence should be addressed. E-mail: vnemykin@d.umn.edu; rodion@imr.edu.
† University of Minnesota at Duluth.
‡ Tohoku University.

including the closed-shell zinc phthalocyanine complex (PcZn), have been recorded at high temperatures in the gas phase,[8,9] in different solvents,[10,11] in cryogenic matrixes at low temperatures,[12] and in supersonic jet expansions.[13] The first spectral assignments of PcZn were provided by Edwards and Gouterman for the gas-phase high-temperature spectra in which the Q, B, N, L, and C (earlier known as M) bands were identified in the UV−vis spectrum.[8] On the basis of PPP-CI calculations, it has been suggested that the Q, B, N, and L bands consist of almost pure $\pi-\pi^*$ single-electron transition configurations,[8] and this idea was dominant for several decades after the original publication until the first band deconvolution analyses for the Q- and B-band regions in UV−vis and MCD spectra of PcZnL complexes (L = pyridine, imidazole, or cyanide ligand located in the axial position of the complex) were presented by Stillman's group in the late 1980s.[10] The simultaneous analysis of UV−vis and MCD spectra in the Q-band region (~1.49−2.48 eV) agreed well with the previously proposed model, while that conducted for the B-band energy envelope (2.85−4.09 eV) revealed two doubly degenerated states labeled as B1 and B2 that were represented by MCD Faraday *A*-terms. In 1995, the same group provided a similar analysis for the low-temperature UV−vis and MCD spectra of the [PcZn(CN)]⁻ complex, although this time the B-band region was deconvoluted using five nondegenerate electronic transitions that were represented in MCD spectra by Faraday *B*-terms.[14] The change in degeneracy of the initial ^1E_u excited state was explained on the basis of Jahn−Teller splitting. This explanation was later questioned by Ricciardi et al. on the basis of time-dependent density functional theory (TDDFT) calculations.[15] Finally, very recently the same group again adopted a "two doubly degenerate" states model in the room-temperature UV−vis and MCD band deconvolution analysis of the substituted PcZn complex.[16] A similar UV−vis and MCD band deconvolution analysis provided by VanCott et al. for the PcZn complex isolated in an argon matrix reveals the presence of at least three electronic transitions (with at least one being vibronically coupled) in the B-band region.[12] Although both research groups agree that the B-band energy envelope should consist of several electronic transitions, the number and nature of excited states located in this region remains uncertain. Another unanswered question belongs to the presence of an electronic transition in the Q_{0-2} vibronic region. An accurate UV−vis and MCD analysis of this spectral envelope[12] suggests the presence of a weak electronic transition, which has never been confirmed computationally.

To gain insight into the nature of the excited states located in the Q- and B-band regions of UV−vis and MCD spectra of PcZn, PPP-CI[8] and numerous semiempirical (primarily ZINDO/S)[17] calculations were conducted by several research groups during the last two decades. In spite of the excellent agreement between the nature and the composition of the most prominent low-energy Q-band observed at ca. 1.86 eV, all of these methods fail to accurately predict the nature, energy, and composition of higher-energy transitions observed in the B-band region. Recently, the TDDFT approach has been suggested as an accurate method for the calculation of vertical excitation energies in organic and inorganic compounds.[18] The TDDFT methodology provides a good compromise between accuracy and computational efficiency as compared to the computationally more expensive CASSCF,[19] MRCI,[20] and SAPT[21] approaches. In TDDFT, the entire spectrum is calculated in a single run, and the computational costs are lower than those of the high-level ab initio methods.[22] Also, an extended basis set is often not required. The applicability of TDDFT for calculating the

vertical excitation energies of porphyrins and related compounds has been recently described in the literature.[15,23] Moreover, several papers on the calculation of electronic spectra of transition-metal phthalocyanines, including PcZn, using the TDDFT approach coupled with pure or hybrid DFT exchange-correlation functionals have been published very recently, and in general, the agreement between experimental observations and calculated UV−vis spectra was better in the case of TDDFT calculations in comparison to semiempirical approaches.[15,23,24] In spite of the significant improvement in the prediction of vertical excitation energies using TDDFT methods, the reliability of such calculations was questioned in a very recent review,[25] mostly due to the disagreement between proposed band deconvolution models and transition energies calculated by the TDDFT method for the B-band energy envelope. Another interesting observation for TDDFT calculations on the PcZn complex is that the calculated energy of the Q-band has always been significantly overestimated. One of the possible reasons for this observation can be a solvent effect. This effect was not considered earlier in TDDFT calculations.[15,23,24] More importantly, all TDDFT calculations conducted on PcZn and its analogues utilized either the pure local spin density approximation (LSDA) or the hybrid B3LYP exchange-correlation functional, while the influence of the type of exchange-correlation functional, and in particular, the amount of Hartree−Fock exchange on the calculated vertical excitation energies have never been targeted.

In this paper, we provide a detailed investigation of the influence of molecular geometry, type of exchange-correlation functional (in sight of the amount of Hartree−Fock exchange involved in the calculation), and solvent effect on the calculated vertical excitation energies in PcZn. The major question that we address is whether or not modern TDDFT or polarized continuum TDDFT model (PCM-TDDFT) methods can accurately predict vertical excitation energies in aromatic macrocyclic systems. To compare theoretical results with experimental ones, we also conducted band deconvolution analyses of UV−vis and MCD spectra of highly soluble zinc tetra-*tert*-butylphthalocyanine in the absence of any axial ligands while taking into consideration vertical excitation energies predicted by TDDFT for PcZn.

Experimental Section

Materials. Zinc tetra-*tert*-butylphthalocyanine (Pc'Zn) was prepared using the literature procedure from commercially available 4-*tert*-butyl phthalonitrile.[26] Another sample of Pc'Zn was purchased from Aldrich Chemical Co. Both samples show the same UV−vis and MCD spectra in the 250−1100 nm spectral region.

Computational Details. All geometries were optimized at the DFT or semiempirical levels. The following methods and basis sets were used in the case of DFT geometry optimization: (i) Becke's pure exchange functional[27] coupled with Perdew's correlation functional[28] (BP86); (ii) Becke's three-parameter hybrid exchange functional[29] coupled with the Lee−Yang−Parr nonlocal correlation functional[30] (B3LYP); (iii) Perdew, Burke, and Ernzerhof's exchange functional along with their 1996 gradient-corrected correlation functional (PBE1PBE).[31] In all cases the standard 6-31G and 6-31G(d) basis sets[32] on zinc and all other atoms, respectively, were used. To investigate solvatochromic effects in PcZn, molecular geometries were again optimized using the above-mentioned exchange-correlation functionals and basis sets, coupled with a self-consistent reaction field method (SCRF), specifically, Tomasi's PCM,[33] in cyclo-

TDDFT and PCM-TDDFT in Phthalocyanines

J. Phys. Chem. A, Vol. 111, No. 50, 2007 **12903**

TABLE 1: Comparison Between X-ray Crystallographically Determined and Optimized Bond Distances and Angles in PcZn

method	Zn−N	N−C_α	C_α−N_{meso}	C_α−C_β	C_β−C_β	C_α−N_{Zn}−C_α	C_α−N_{meso}−C_α
BP86/gas phase	1.994	1.385	1.339	1.466	1.420	109.0	123.8
B3LYP/gas phase	1.990	1.373	1.330	1.461	1.410	109.4	124.3
PBE1PBE/gas phase	1.982	1.366	1.326	1.456	1.405	109.4	124.2
ZINDO/1	1.980	1.381	1.346	1.452	1.424	107.0	125.4
experimental[a]	1.980(2)	1.369(2)	1.331(2)	1.455(2)	1.400(3)	109.1(2)	123.5(2)

[a] Data from ref 52.

hexane, benzene, methylene chloride, and dimethyl sulfoxide. In all cases, frequency calculations were done on optimized structures to confirm the local minima. DFT-predicted geometries of PcZn were used in TDDFT or PCM-TDDFT calculations of vertical excitation energies using the exchange-correlation functionals mentioned in the tables and figures below and 6-31G and 6-31G(d) basis sets on zinc and all other atoms, respectively. The choice of basis set belongs to the earlier observation of the similarity between the calculated vertical excitation energies in porphyrinoid compounds for 6-31G(d), 6-31G+(d), and 6-311+G(d) basis sets.[23] In the case of the SCRF PCM model, TDDFT calculations were conducted using both nonequilibrium and equilibrium PCM solvation methods. The lowest 40 vertical excitation energies were considered in the case of all TDDFT calculations. At the semiempirical level, vertical excitation energies in PcZn were calculated using ZINDO/S[34] and PM3[35] approaches considering all excitations with energies lower than 9 eV. To test the effect of the $\pi-\pi$ weighting factor on predicted transition energies in the ZINDO/S method, three separate sets of calculations were performed on the DFT- and ZINDO/1-predicted geometries with $\pi-\pi$ weighting factors of 0.585, 0.640, and 0.649 (see Results and Discussion section). All DFT and TDDFT calculations were performed using the Gaussian 03 program,[36] while all semiempirical calculations were conducted using HyperChem 7.5 software.[37] The atomic orbital contributions to their respective molecular orbitals in PcZn were calculated using the VMOdes program.[38]

UV−Vis and MCD Spectra. Room-temperature UV−vis data were obtained on HP 8453 or Cary 17 spectrophotometers using the appropriate solvents, which are indicated in the Results and Discussion section. In all cases, spectra were recorded in a 235−900 nm spectral region with a data density of 1 nm per point. MCD data were recorded using an OLIS DSM 17 CD spectropolarimeter operating under OLIS GlobalWorks software using a 1.4 T DeSa magnet. Spectra were recorded in dichloromethane within a 235−900 nm spectral range. A data density of 0.5 nm per point was used along with a 2 nm bandwidth and 0.4 s per data point. Four scans were averaged for data sets acquired in parallel and antiparallel magnetic field alignments. Final MCD spectra were smoothed using the fast Fourier transform digital filter available in GlobalWorks software provided by OLIS Inc.

Band Deconvolution Analysis. UV−vis and MCD spectra of the Pc^{r}Zn complex were deconvoluted separately in both Q- and B-band spectral envelopes using a global fit procedure. The Origin 7.5 Pro program[39] and Gaussian spectroscopic functions were used in all cases. MCD Faraday *B*-terms were modeled by Gaussian spectroscopic functions with positive or negative amplitudes implemented into the Origin software. MCD Faraday *A*-terms were modeled as a sum of negative and positive Gaussian functions of equal amplitude and bandwidth. UV−vis spectra of Pc^{r}Zn were deconvoluted using Gaussian functions. In the case of global fits of UV−vis and MCD data, the UV−vis and MCD band baricenters and bandwidths were kept

fixed, while band amplitudes were allowed to be adjusted to obtain the best fit.

Results and Discussion

Optimized Molecular Geometries of PcZn in the Gas Phase and Solution. All geometry optimizations on PcZn were performed using D_{4h} symmetry[40] with the most important bond distances and angles for the gas phase and semiemperical and solution optimized geometries listed in Table 1 and Supporting Information Table 1, respectively, while the labeling scheme is presented in Figure 1. Geometries optimized in solution varied by less than 0.01 Å from their respective gas-phase-optimized geometries in all cases. To compare the influence of PcZn molecular geometry in the gas phase and solution on the calculated vertical excitation energies, we performed geometry optimizations using a pure (BP86) and two hybrid (B3LYP and PBE1PBE) exchange-correlation functionals. We chose these three functionals with 0%, ~20%, and ~25% of Hartree−Fock exchange because it was recently pointed out that the optimized bond distances and angles in metallocomplexes correlate with the amount of Hartree−Fock exchange involved in the calculations.[18,41,42] In agreement with this trend, the optimized bond distances in the gas phase for PcZn become shorter when the amount of Hartree−Fock exchange incorporated into the exchange-correlation functional increases. The bond length changes, however, are small (~0.01 Å) and, as it will be shown below, do not significantly affect the calculated vertical excitation energies in PcZn. Similar bond distance and angle deviations in the PcZn complex were predicted in solution (Supporting Information Table 1). The overall agreement between optimized and experimentally determined structures of PcZn[40] is excellent for DFT optimizations, while use of the ZINDO/1 Hamiltonian leads to a significant difference between calculated and experimentally observed angles in PcZn.

Ground-State Electronic Structure of PcZn as a Function of Exchange-Correlation Functional. In general, it was found that the influence of the starting geometry on the calculated electronic structure of PcZn is smaller in comparison to the difference caused by the exchange-correlation functional used in DFT calculations or the employed semiempirical method. Thus, only calculations based on the B3LYP-optimized geometry will be discussed in detail, although all data are listed in
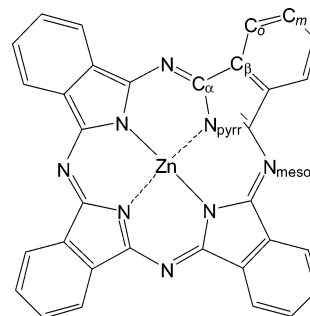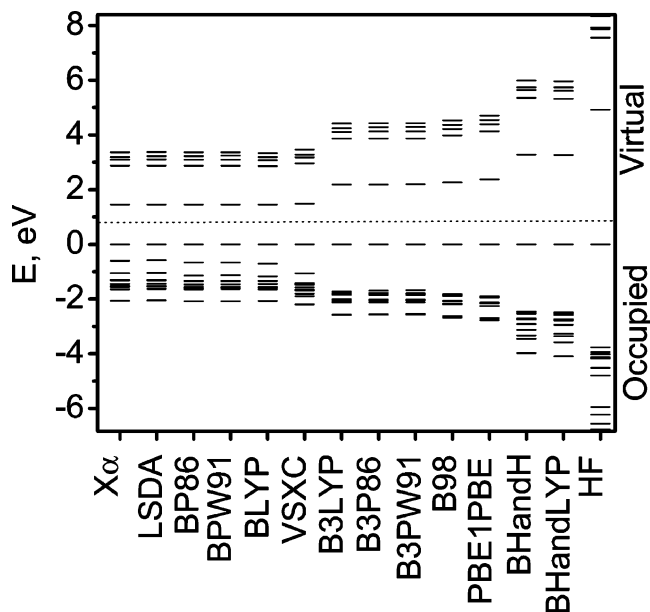

Figure 1. Labeling scheme in PcZn.

Figure 2. Partial molecular orbital diagram of PcZn calculated at the DFT level of theory. The HOMO ($2a_{1u}$) energy is normalized to 0 eV.
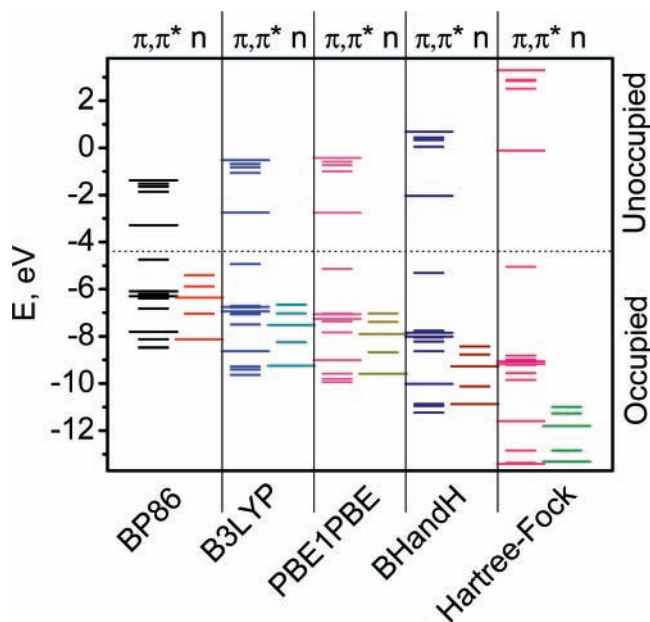

Figure 3. Relative energies of π- and n-type molecular orbitals in PcZn calculated at the DFT level of theory using pure (BP86), hybrid (B3LYP and PBE1PBE), and "half-and-half" hybrid (BHandH) exchange-correlation functionals along with the Hartree−Fock level of theory.

Supporting Information Tables 2 and 3. The frontier molecular orbital diagrams and frontier molecular orbital compositions calculated using a B3LYP-optimized geometry and 14 different exchange-correlation functionals are shown in Figure 2 and are listed in Supporting Information Table 2, respectively, while the typical expanded molecular orbital diagrams for a pure exchange-correlation functional, two hybrid exchange-correlation functionals, a "half-and-half" hybrid exchange-correlation functional, and the Hartree−Fock method are presented in Figure 3. In all cases, zinc d_{xy}, d_{z^2}, d_{xz}, and d_{yz} orbitals have very low energies, and because they do not participate in electronic transitions observed in the Q- and B-band spectral envelopes, we will not discuss these below. The metal-centered $d_{x^2-y^2}$ orbital, however, has a significant contribution in the predominantly pyrrolic nitrogen-centered nonbonding $11b_{1g}$

molecular orbital. The importance of this nonbonding orbital in $n \rightarrow \pi^*$ transitions will be discussed in the next section.

The phthalocyanine π-system consists of 32 carbon and 8 nitrogen atoms and involves 42 electrons distributed over 21 occupied molecular π-orbitals. In addition, 19 unoccupied molecular π-orbitals can, at least theoretically, participate in $\pi-\pi^*$ transitions in PcZn. As an example, all 40 π-orbitals calculated using a B3LYP exchange-correlation functional and the ZINDO/S semiempirical method are depicted in Supporting Information Figures 1 and 2, while those playing an important role in the formation of the absorption spectrum of PcZn in the Q- and B-band regions are shown in Figure 4. According to the classic Gouterman's four-orbital model,[8] the frontier molecular orbitals should be π-orbitals of a_{1u}, a_{2u} (both occupied), and e_g (unoccupied) symmetries. In all DFT and semiempirical calculations tested, the highest occupied molecular orbital (HOMO) is indeed represented by a $2a_{1u}$ π-orbital, while the lowest unoccupied molecular orbital (LUMO) consists of degenerate $7e_g$ π-orbitals, which is in agreement with the classic Gouterman's four-orbital orbital scheme description. Both the HOMO and the degenerate LUMO are energetically well-separated from the other occupied and unoccupied molecular orbitals, respectively. In excellent agreement with the earlier observations,[42] the HOMO−LUMO energy gap calculated at the DFT level linearly correlates with the amount of Hartree−Fock exchange involved in the calculations (Figure 5). Also, the position of the $5a_{2u}$ π-orbital in Gouterman's model (we will use the $5a_{2u}$ orbital, which is the closest to the HOMO, as representing Gouterman's description, although, as it was pointed out by Ricciardi et al., the situation is more complicated)[15] strongly depends on the employed exchange-correlation functional or semiempirical method. Indeed, in the case of the semiempirical PM3 and ZINDO/S methods, the a_{2u} symmetry molecular orbital is HOMO − 1 as expected from Gouterman's four-orbital model. A similar situation was also observed for Hartree−Fock calculations as well as "half-and-half" (BHandLYP and BHandH) hybrid exchange-correlation functionals, which involve 50% of Hartree−Fock exchange. A decrease in the amount of Hartree−Fock exchange involved in the DFT calculations below 25%, however, results in a significant stabilization of the $5a_{2u}$ orbital in comparison to the $3b_{2u}$ and $6e_g$ π-orbitals as well as the $11b_{1g}$ and $9b_{2g}$ nitrogen lone-pair-based n-orbitals. As a result, the $5a_{2u}$ orbital becomes HOMO − 5 in the case of all tested hybrid exchange-correlation functionals and HOMO − 6 in the case of pure exchange-correlation functionals (Supporting Information Tables 2 and 3). More interestingly, all DFT calculations with pure and hybrid (25% or less Hartree−Fock exchange admixture) exchange-correlation functionals indicate the presence of a $3b_{2u}$ symmetry π-orbital between Gouterman's $2a_{1u}$ (HOMO) and $5a_{2u}$ π-orbitals. The presence of this orbital results in a $3b_{2u} \rightarrow 7e_g$ (LUMO) symmetry-allowed transition with a lower excitation energy than that of the $5a_{2u} \rightarrow 7e_g$ (LUMO) transition, which will be discussed in the next section. Also interesting, the relative energies of $3b_{2u}$ and $5a_{2u}$ as well as Gouterman's $2a_{1u}$ and $5a_{2u}$ orbitals again linearly correlate with the amount of Hartree−Fock exchange involved in the calculation (Figure 5). The slopes of these two correlation lines, however, are different, which results in a crossover between energies of the $3b_{2u}$ and $5a_{2u}$ orbitals (Figure 5).

The most important (for the description of the Q- and B-band region of UV−vis and MCD spectra of PcZn) n-orbitals are the $11b_{1g}$, $9b_{2g}$, $19e_u$, $13a_{1g}$, and $18e_u$ molecular orbitals (Supporting Information Table 3 and Figures 3 and 6). A
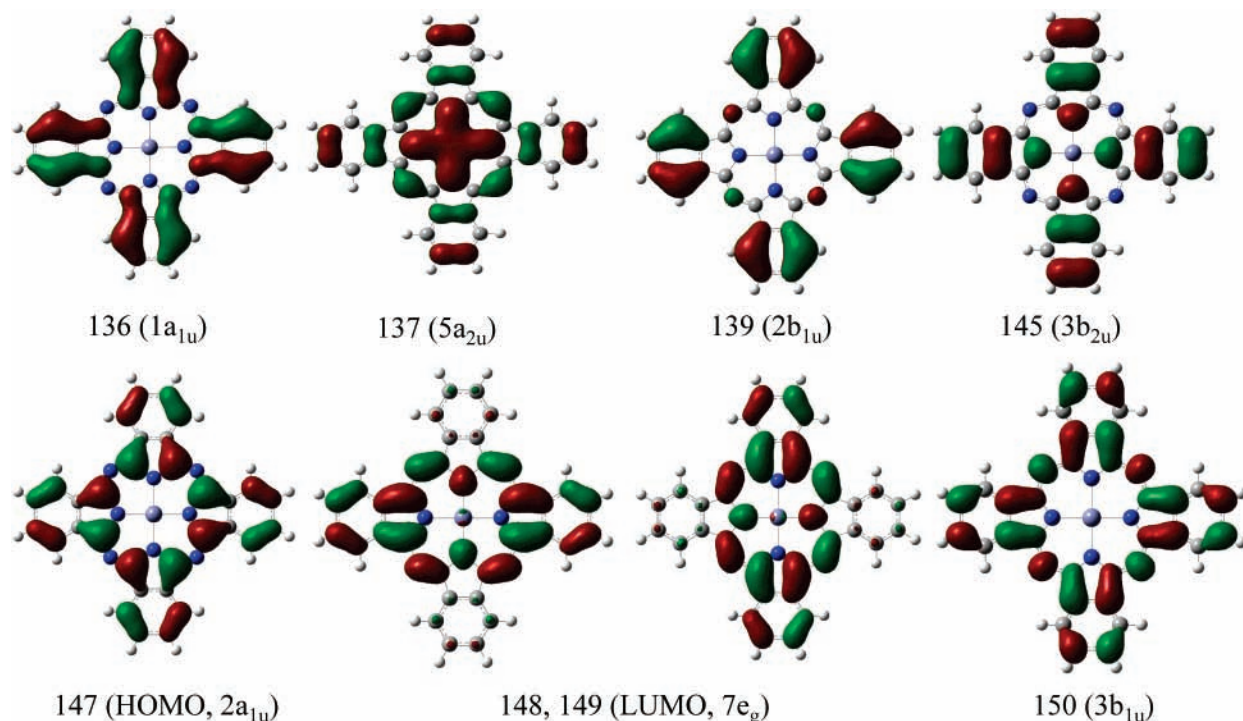
TDDFT and PCM-TDDFT in Phthalocyanines

J. Phys. Chem. A, Vol. 111, No. 50, 2007 **12905**

Figure 4. Frontier π-orbitals calculated at the DFT level of theory using the B3LYP exchange-correlation functional.

"Hartree–Fock exchange dependency" similar to that observed in the case of π-orbitals- was also observed in the case of the predominantly nitrogen-based lone pair orbitals (Figure 3). For instance, the energy difference between $2a_{1u}$ (HOMO) and the highest energy n-type ($11b_{1g}$) orbitals linearly correlates with the amount of Hartree–Fock exchange involved in the calculation (Figure 7). Indeed, the predominantly pyrrolic nitrogen-based $11b_{1g}$ orbital is actually HOMO − 1 when pure exchange-correlation functionals were employed for the calculations, while a significant stabilization of its energy was observed when nonzero Hartree–Fock exchange was involved in the calculations. The major difference between the semiempirical and the pure or hybrid DFT calculations is the relative energies of nitrogen n-orbitals with respect to phthalocyanine π-orbitals (Figure 8). Indeed, n-orbitals were predicted to be significantly more stable in the case of semiempirical, "half-and-half" hybrid DFT, and pure Hartree–Fock calculations in comparison to their energies calculated using pure or hybrid DFT exchange-correlation functionals. In the latter case, relatively high-energy nitrogen-based n-orbitals can result in a low-energy, symmetry-forbidden, but vibronically allowed transition, which will be discussed in the next section.

It is interesting to compare the DFT-calculated energies of occupied molecular orbitals with the experimental UV photoelectron spectroscopy (UPS) spectrum of PcZn (Figure 9).[43] It seems that all hybrid DFT exchange-correlation functionals, probably, provide the best agreement between theory and the well-known four-peak experimental ionization energy profile. The molecular orbital energies calculated using pure exchange-correlation functionals also agree well with experiment except in the second peak area observed in the UPS spectrum of PcZn, while the agreement between the molecular orbital energies calculated at "half-and-half" hybrid, Hartree–Fock, and semiempirical levels of theory and the experimental UPS spectrum is significantly poorer. Finally, it was found that the electronic structures of PcZn calculated in the gas phase and solution at the same level of theory are very similar to each other and thus will not be discussed in detail.

TDDFT- and PCM–TDDFT-Predicted Vertical Excitation Energies of PcZn in the Q- and B-Band Energy Regions. The major goal of this paper is to find out whether or not modern TDDFT methods can accurately describe vertical excitation energies in complex transition-metal molecules and, in particular, PcZn. Experimental UV–vis and MCD spectra of Pc^{t}Zn are shown in Figure 10. Following the current classification,[12,17,25] they can be divided into Q, B, N, L, and C regions, out of which only the Q ($\sim$1.49–2.23 eV) and B ($\sim$2.85–4.09 eV) band spectral envelopes will be discussed in detail. In the UV–vis spectrum of Pc^{t}Zn, the Q-band region consists of a single intense band observed at 1.83 eV (677 nm), known as the Q_{0-0} transition.[6] This is followed by two bands at 1.91 (648 nm) and 2.03 eV (612 nm), which are usually described as Q_{0-1} and Q_{0-2} vibronic satellites of the electronic Q_{0-0} transitions.[6] In the MCD spectrum of Pc^{t}Zn, the Q_{0-0} band is represented by a Faraday MCD *A*-term centered at 1.83 eV (677 nm), while the Q_{0-1} and Q_{0-2} vibronic satellites are represented by Faraday MCD *B*-terms that are observed at 1.93 eV (644 nm) and 2.02 eV (613 nm), respectively. The B-band energy envelope (2.73–4.22 eV) in the UV–vis spectrum of Pc^{t}Zn is represented by a broad asymmetric band centered at 3.57 eV (347 nm, Figure 10). This band can be seen as a Faraday pseudo-*A*-term centered at 2.58 eV (346 nm) in the MCD spectrum of Pc^{t}Zn. We will keep this simple description of the UV–vis and MCD spectra of Pc^{t}Zn in the Q- and B-band regions in this section, while a detailed deconvolution analysis will be discussed later in this paper.

TDDFT Gas-Phase Calculations. Vertical excitation energies for the Q- and B-band regions of the UV–vis and MCD spectra of Pc^{t}Zn, listed in Supporting Information Tables 4 and 5 and shown graphically in Figure 11, were calculated using a B3LYP-optimized geometry and 14 different exchange-correlation functionals. Similar to the molecular orbital energies discussed in the previous section, the calculated vertical excitation energies in PcZn show a prominent dependency on the amount of Hartree–Fock exchange involved in the TDDFT calculations (Figure 11). Overall, only vertical excitation energies calculated
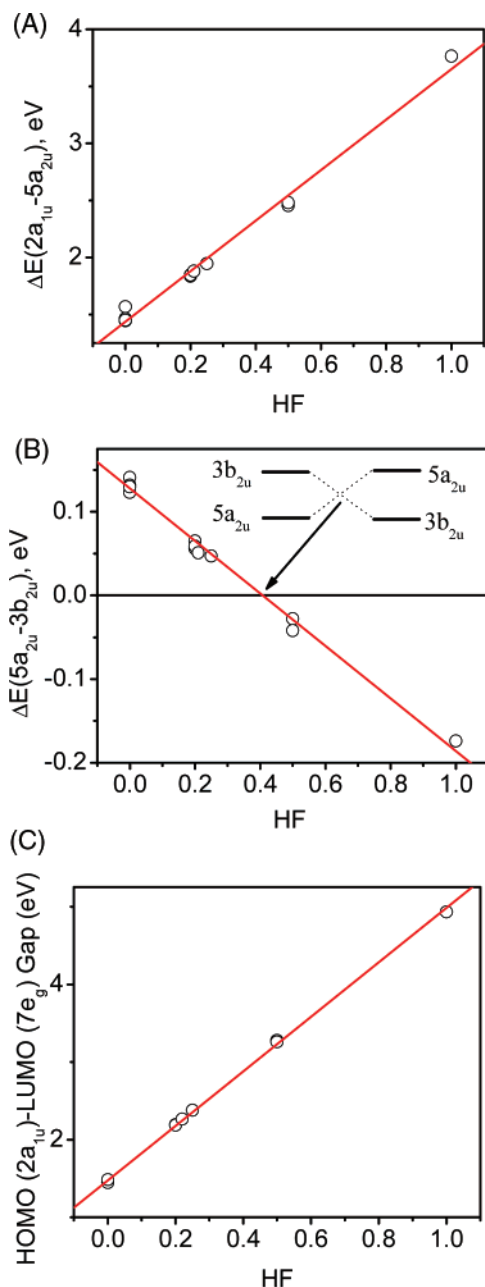
Figure 5. Linear correlation between energy difference of Gouterman's (A) $2a_{1u}$ and $5a_{2u}$, (B) $5a_{2u}$ and $3b_{2u}$, and (C) HOMO and LUMO orbitals calculated at the DFT level of theory as a function of the amount of Hartree−Fock exchange involved in the calculation.

using pure or hybrid exchange-correlation functionals provide an acceptable agreement with experimental data, while those calculated using "half-and-half" hybrid exchange-correlation functionals or at Hartree−Fock levels of theory significantly overestimate the transition energies. Next, a detailed analysis of TDDFT-calculated vertical excitation energies of PcZn clearly indicates that all results from pure and hybrid exchange-correlation functionals can be combined into two separate groups. Taking these groups into consideration and for the sake of simplicity, a detailed analysis of vertical excitation energies calculated using BP86 (pure exchange-correlation functional), B3LYP (hybrid exchange-correlation functional with ∼20% of Hartree−Fock exchange), and PBE1PBE (hybrid exchange-correlation functional with ∼25% of Hartree−Fock exchange) functionals is provided in Supporting Information Table 4, while a complete comparative data set for all 14 exchange-correlation

functionals is shown in Figure 11 and tabulated in Supporting Information Table 5.

In excellent agreement with the experimental data, only one symmetry-allowed transition was predicted by the TDDFT method in the case of the Q-band spectral envelope of PcZn. Also in agreement with previously reported PPP,[8] semiempirical,[17] and TDDFT calculations[15,23,24] and in all cases, the Q_{0-0} transition can be described as a configurationally almost pure electron excitation from $2a_{1u}$ (HOMO) to $7e_g$ (LUMO, Supporting Information Figure 3). All tested pure, hybrid, and "half-and-half" hybrid DFT exchange-correlation functionals slightly overestimate the vertical excitation energy of the predominantly $2a_{1u} \rightarrow 7e_g$ 1^1E_u excited state with errors of 0.16−0.21, 0.26−0.29, and 0.23−0.27 eV observed for the pure, hybrid, and "half-and-half" hybrid exchange-correlation functionals, respectively. Analysis of these errors indicates a slightly better performance of pure exchange-correlation functionals, although the error ranges seen here are typical for the TDDFT approach and should be considered as a good agreement between theory and experiment. Interestingly, the time-dependent Hartree−Fock method underestimates the vertical excitation energy of the first excited state in PcZn by 0.25 eV.

The situation becomes more complicated when the B-band spectral envelope is considered. Indeed, all pure exchange-correlation functionals except vanVoorhis and Senserian's τ-dependent functional (VSXC)[44] predict eight symmetry-allowed electronic transitions in the B-band area (Supporting Information Table 5 and Supporting Information Figure 3), and these transitions are similar to those calculated by Ricciardi et al. using the LSDA exchange-correlation functional and Slater-type basis functions.[15] Out of these excitations, the six most intense belong to $\pi \rightarrow \pi^*$ transitions, while two transitions with low intensity can be clearly attributed to $n \rightarrow \pi^*$ transitions. The lowest vertical excitation energy transition calculated in the B-band region is $\pi \rightarrow \pi^*$ in nature and predominantly belongs to the excitation of an electron from the $3b_{2u}$ orbital to the $7e_g$ (LUMO) orbital. This transition has relatively low intensity and is very important in the band deconvolution analysis of UV−vis and MCD spectra of Pc'Zn presented in the next section. The next group of excited states includes two $\pi \rightarrow \pi^*$ transitions and one $n \rightarrow \pi^*$ transition (Supporting Information Table 5 and Figure 11). The major contributions into the 3^1E_u and 4^1E_u excited states originate from the electron excitations from the $5a_{2u}$ and $2b_{1u}$ orbitals to LUMO. The first symmetry-allowed $^1A_{2u}$ excited state was calculated between 3.07 and 3.16 eV and, as expected, has a low intensity. The next calculated excited state (5^1E_u) belongs to the symmetry-allowed, predominantly $2a_{1u} \rightarrow 8e_g$ $\pi-\pi^*$ transition. 6^1E_u and 7^1E_u excited states have the highest TDDFT-calculated oscillator strengths in the B-band region and predominantly originate from $1a_{1u}$ or $4a_{2u}$ electron excitations to $7e_g$ orbitals. Finally, the energy of the 2^1A_{2u} excited state was calculated close to 7^1E_u. Similar excited states were calculated using the τ-dependent VSXC exchange-correlation functional, except the 2^1A_{2u} excited state has an energy outside of the B-band region. In the case of all tested hybrid exchange-correlation functionals, six symmetry-allowed excited states were predicted in the B-band spectroscopic envelope, which in general have higher energies in comparison to those calculated using pure exchange-correlation functionals. The first four excited states follow the same order as in the case of pure exchange-correlation functionals. The calculated energies of 5^1E_u and 6^1E_u excited states, however, are switched in comparison to those calculations utilizing pure exchange-correlation functionals. Finally, "half-and-half" hybrid
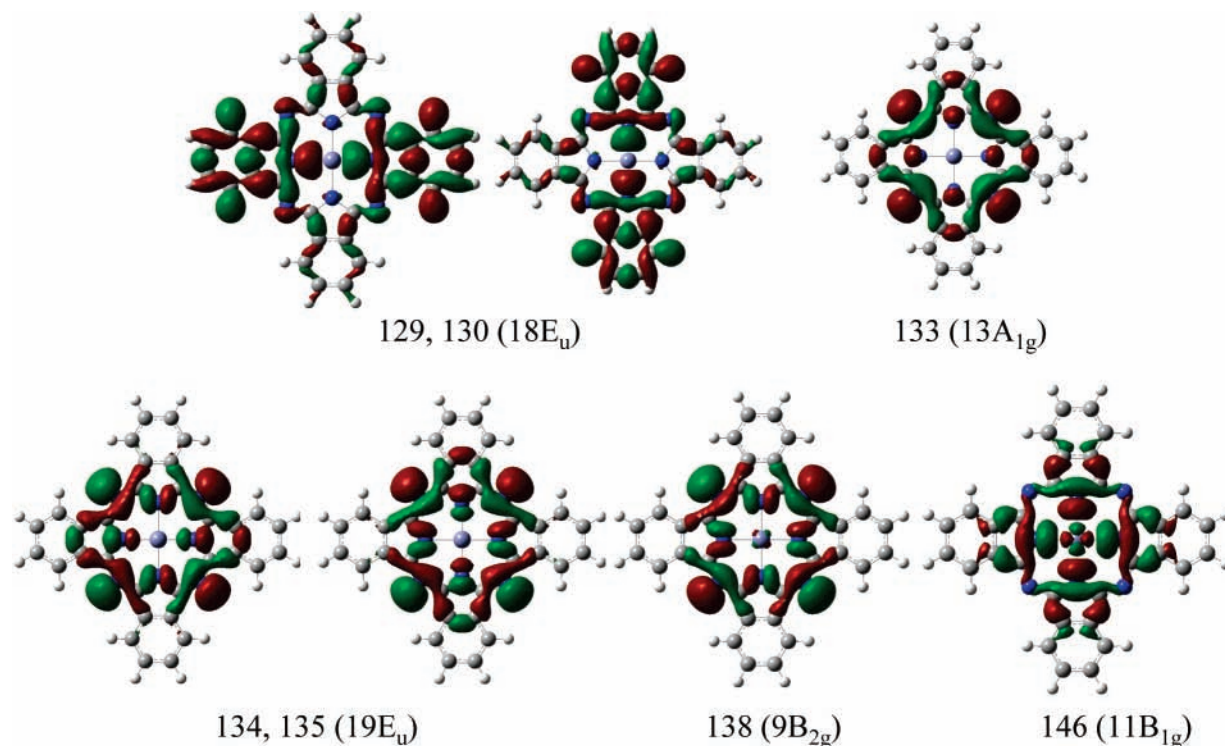
TDDFT and PCM-TDDFT in Phthalocyanines

J. Phys. Chem. A, Vol. 111, No. 50, 2007 **12907**

129, 130 (18E$_u$)   133 (13A$_{1g}$)

134, 135 (19E$_u$)   138 (9B$_{2g}$)   146 (11B$_{1g}$)

Figure 6. Frontier n-type molecular orbitals calculated for PcZn at the DFT level of theory using the B3LYP exchange-correlation functional.
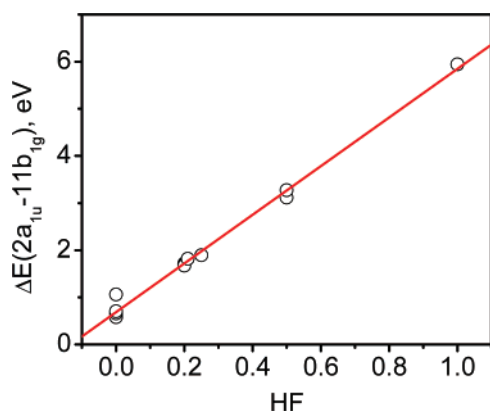

Figure 7. Linear correlation between the energy differences of 2a$_{1u}$ and 11b$_{1g}$ orbitals calculated at the DFT level of theory.

Figure 8. Relative energies of π- and n-type molecular orbitals in PcZn calculated at the semiempirical level of theory

exchange-correlation functionals as well as the time-dependent Hartree−Fock approach significantly overestimate vertical excitation energies for the transitions located in the B-band region.

To investigate the influence of the starting geometry of PcZn on the calculated vertical excitation energies, we conducted TDDFT calculations using one pure (BP86) and two hybrid (B3LYP and PBE1PBE) exchange-correlation functionals on two additional molecular geometries of PcZn optimized using BP86 and PBE1PBE exchange-correlation functionals. It was found that, although present, the effect of starting geometry (when the same exchange-correlation functional was used in TDDFT calculations) is rather small with typical deviations of calculated vertical excitation energies of 0.03−0.05 eV. Interestingly, the shortening of bond distances upon going from the BP86-optimized geometry to B3LYP- and then to PBE1PBE-optimized geometries results in a monotonic increase in the TDDFT-calculated vertical excitation energies with the best agreement between the experimental and the calculated Q-band position observed when pure exchange-correlation functionals
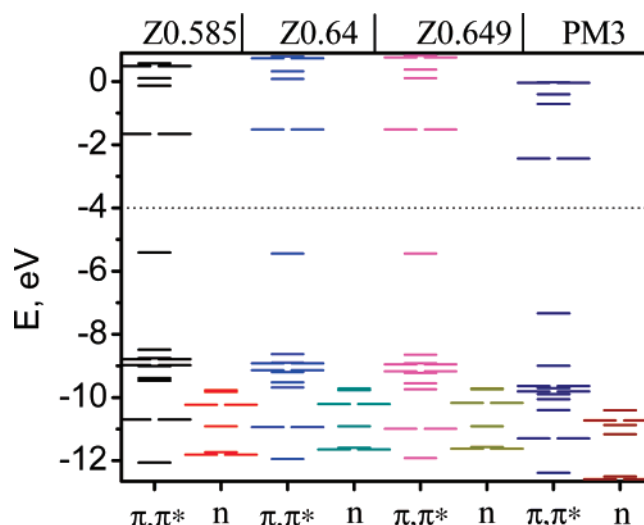
were used for TDDFT calculations on the BP86-optimized geometry (Figures 11 and 12).

PCM-TDDFT Calculations. It is well-known that the parameters in the semiempirical methods traditionally used in the modeling of excited states of phthalocyanines already include, to some extent, solvent−solute interactions.[45] However, solvent effects are not included in the gas-phase TDDFT calculations. Inclusion of solvent effects in TDDFT calculations can significantly improve the agreement between the experimental and the predicted vertical excitation energies in transition-metal complexes.[46] Thus, it would be interesting to determine the extent of solvent influence on the TDDFT-predicted vertical excitation energies in PcZn. To clarify such an influence, we calculated vertical excitation energies of PcZn using BP86, B3LYP, and PBE1PBE exchange-correlation functionals in several solvents. In each case, the geometry of PcZn was
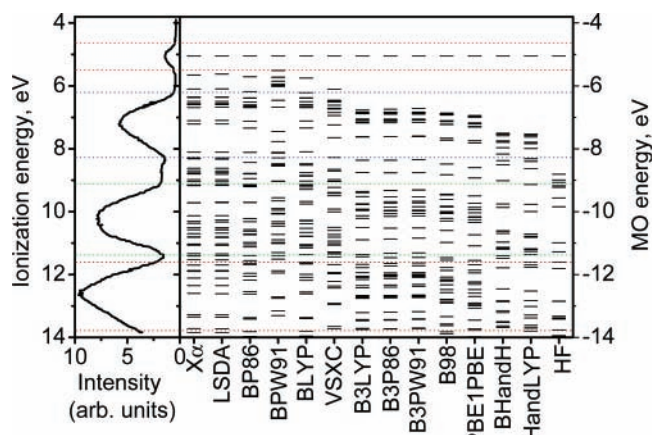
Figure 9. Relative energies of molecular orbitals calculated for PcZn at the DFT level theory. The energy of the HOMO is adjusted to the position of the first peak observed in the UPS spectrum. The UPS spectrum is adapted from ref 43.
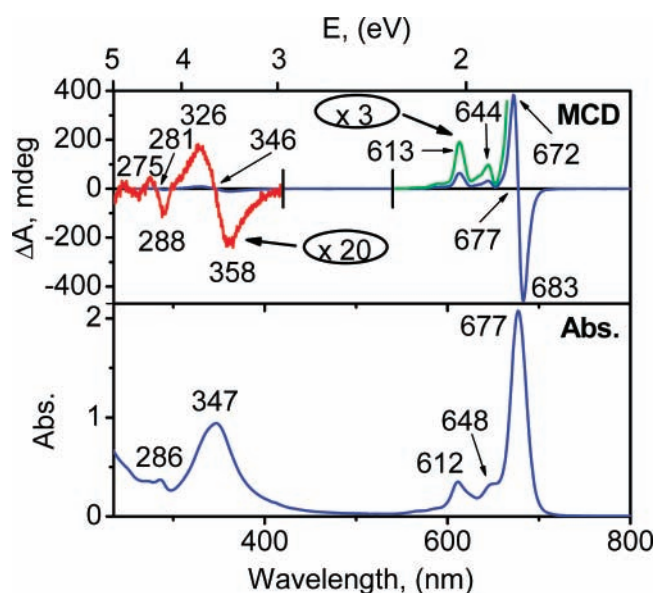

Figure 10. Room-temperature experimental MCD and UV−vis spectra of Pc'Zn (10^{-5} mol/L) recorded in dichloromethane.
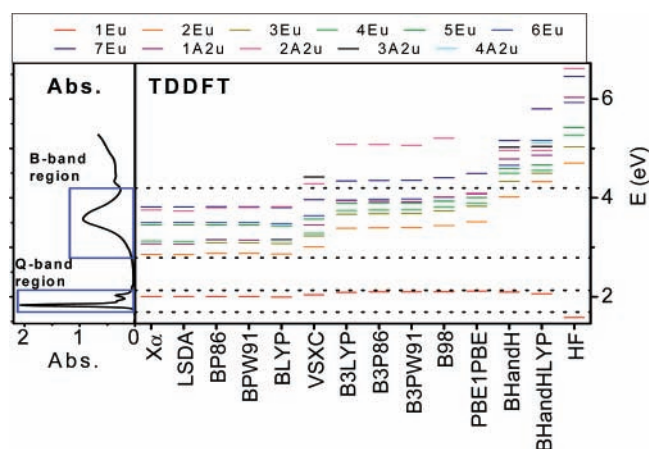

Figure 11. Comparison between gas-phase TDDFT-predicted vertical excitation energies of PcZn and the experimentally observed UV−vis spectrum of Pc'Zn in dichloromethane.

optimized using the PCM approach[33] coupled with the same exchange-correlation functional used in PCM-TDDFT calculations. The results of these PCM-TDDFT calculations show
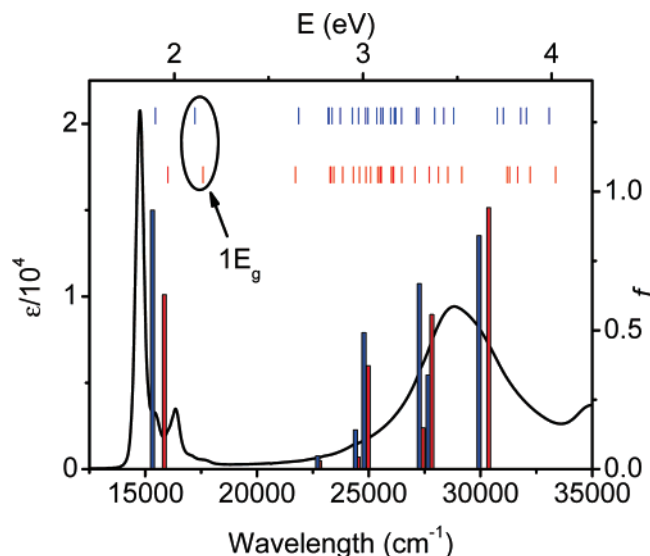

Figure 12. Comparison between gas-phase (red bars) and solution (cyclohexane, blue bars) TDDFT-predicted (BP86 EC functional) vertical excitation energies of PcZn and its experimentally observed UV−vis spectrum. Bars on the top indicate all predicted transitions, while those on the bottom reflect calculated oscillator strengths. The first degenerate symmetry-forbidden n → π* transition is indicated by an arrow.
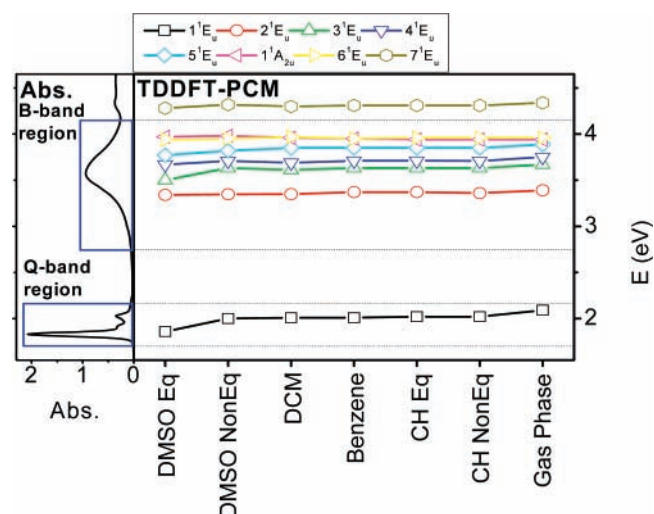

Figure 13. Comparison between gas-phase and PCM−TDDFT-predicted (B3LYP EC functional) vertical excitation energies of PcZn and the experimentally observed UV−vis spectrum of Pc'Zn.

similar trends and are graphically presented in Figures 12 and 13 as well as Supporting Information Figure 4. In all cases tested, an increase of solvent polarity leads to a decrease in the calculated vertical excitation energies and results in a better agreement between theory and experiment. In general, the PCM-TDDFT-predicted solvatochromic effect in PcZn was found to be the largest for the Q-band. In the case of the nonequilibrium PCM-TDDFT approach, the magnitude of the solvatochromic effect calculated for the Q-band (0.01−0.03 eV) is in the perfect agreement with the experimental data (Table 2). In the equilibrium solvation PCM-TDDFT calculations, however, the predicted magnitude of Q-band solvatochromism is slightly overestimated (0.12−0.18 eV). Overall, it seems that PCM-TDDFT calculations do provide, at least for the Q-band, a slightly better agreement between the predicted and the experimentally observed transition energies in comparison to the gas-phase TDDFT approach.

TDDFT and PCM-TDDFT in Phthalocyanines

J. Phys. Chem. A, Vol. 111, No. 50, 2007 **12909**

TABLE 2: Experimental and PCM-TDDFT-Predicted[a] Q-Band Position in Pc'Zn as a Function of Solvent

	experiment		B3LYP	BP86	PBE1PBE
solvent	λ (nm)	E (eV)	E (eV)	E (eV)	E (eV)
hexane[b]	672	1.85	2.02 (2.02)	1.90(1.90)	2.06 (2.06)
toluene	677	1.83	2.01		
dichloromethane	678	1.83	2.01		
DMSO	678	1.83	2.00 (1.86)	1.89 (1.78)	2.03 (1.88)
Δ(hexane − DMSO)		0.02	0.02 (0.16)	0.01 (0.12)	0.03 (0.18)

[a] Equilibrium PCM solvation TDDFT energies are presented in parentheses. *[b]* Cyclohexane was used as a solvent for PCM-TDDFT calculations.

Semiempirical PM3 and ZINDO/S Calculations. Next, it is logical to compare the vertical excitation energies for PcZn calculated using modern TDDFT and PCM-TDDFT methods with those conducted at the semiempirical level. This comparison is especially important due to the fact that the band deconvolution analysis provided by Stillman's group until recently was heavily dependent on the electronic structures and vertical excitation energies calculated using semiempirical methods. In the case of ZINDO/S calculations, we used both recommended $\pi-\pi$ overlap weighting factors (0.585 and 0.64)[47] along with the recently suggested value of 0.649.[48] We included the last $\pi-\pi$ overlap weighting factor because it was claimed that its use significantly improves the agreement between theory and experiment for calculated vertical excitation energies. The energies of all bands calculated using the ZINDO/S method heavily depend on the applied $\pi-\pi$ overlap weighting factor, as expected from the theory of this semiempirical approach. In general, the larger the value of the $\pi-\pi$ overlap weighting factor, the higher the calculated band excitation energy (Supporting Information Table 6). The ZINDO/S-calculated energy of the Q-band consisting of the almost pure $2a_{1u} \rightarrow 6e_g$ transition (note that at the semiempirical level the $6e_g$ orbital set is the LUMO) is in an excellent agreement with experimental data for all three geometries tested as well as TDDFT and PCM-TDDFT calculations. Thus, the largest deviations for the calculated Q-band of 0.023, 0.034, and 0.036 eV for the $\pi-\pi$ overlap weighting factors of 0.585, 0.640, and 0.649, respectively, have been observed for PcZn using a molecular geometry optimized at the B3LYP level (Supporting Information Table 6). The situation is quite different for the agreement between theory and experiment in the case of the higher-energy B-band energy envelope (Figure 14) of the PcZn spectrum. All three tested ZINDO/S approaches for all geometries suggest the presence of only a single band in this area, consisting of a $2a_{1u} \rightarrow 7e_g$ transition, while the expected B1 and B2 bands, consisting predominantly of $2a_{2u} \rightarrow 6e_g$ and $3b_{1u} \rightarrow 6e_g$ transitions, respectively, were calculated between 4.07−4.48 and 4.28−4.71 eV. These calculated energies are outside of the B-band range (Supporting Information Table 6 and Figure 14). The calculated energy of the n $\rightarrow \pi^*$ transition was found between 4.66 and 4.95 eV. Overall, the ZINDO/S method predicts six intense degenerate transitions, which can contribute to the intensity of the B-band region, but it should be pointed out that the large absolute deviations from experimental values make exact band assignments quite speculative. The calculated intensity of the B1 band is significantly overestimated, but taking into consideration that its predicted intensity is way above any other predicted band in this region, it is relatively safe (following assignments suggested by Stillman and co-workers) to assume that the B1 band transition energy is overestimated by 0.327−0.738 eV when the ZINDO/S method is used. This deviation is a lower than the expected accuracy for any accurate computa-
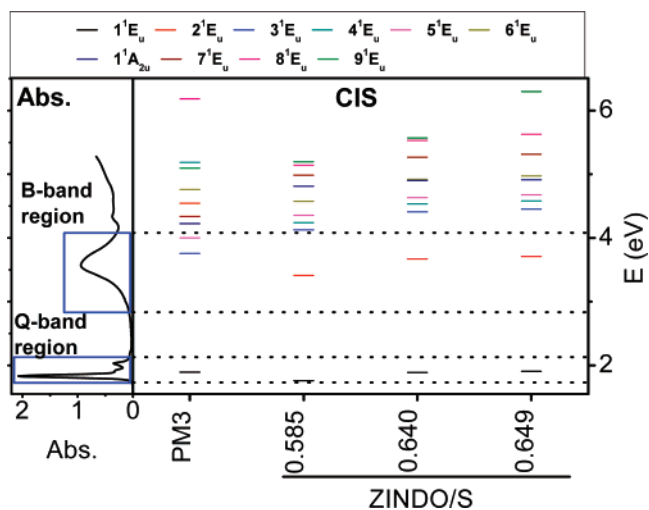

Figure 14. Comparison between the predicted at the semiempirical level of theory vertical excitation energies of PcZn and the experimentally observed UV−vis spectrum of Pc'Zn.

tional method. The assignment of the B2 band on the basis of ZINDO/S calculations is not straightforward. Indeed, four bands with energies between ∼3.35 and 4.96 eV have comparable oscillator strengths and thus can be assigned to the B2 band. The overall performance of the ZINDO/S method in the calculation of the excitation energies in PcZn can be summarized as follows: (i) the Q-band energy can be predicted very accurately using any geometry and $\pi-\pi$ overlap weighting factor tested; (ii) all calculated excitation energies in the UV region are significantly overestimated, making it difficult to assign experimentally observed bands to theoretically predicted transitions; (iii) the average deviation for the whole spectrum of PcZn primarily depends on the value of the $\pi-\pi$ overlap weighting factor used, while the influence of starting geometry is relatively small; (iv) unlike suggested earlier,[48] an increase in the value of the $\pi-\pi$ overlap weighting factor significantly shifts the energies of UV bands, worsening the agreement between theory and experiment.

The overall performance of the NDDO-based PM3 method is slightly better in comparison to the INDO-based ZINDO/S approach (Supporting Information Table 6). Indeed, in this case, not only the Q-band, but also the B1 and B2 band positions are acceptably close to experimental values, although, as it will be discussed below, it is hard to believe that the B-band spectral envelope consists of only two electronic transitions.

UV−Vis and MCD Band Deconvolution Analysis: Comparison between Theory and Experiment. The reliability of TDDFT methods for the calculation of vertical excitation energies in inorganic, organometallic, and macrocyclic systems was widely discussed in the literature,[18] and with respect to the application of these methods to phthalocyanines and their analogues, two opinions are currently present. Ricciardi et al. advocate use of modern TDDFT methods for the calculation of the vertical excitation energies in phthalocyanines, based on an excellent agreement between calculated transitions and prominent absorption bands observed for PcZn.[15] Their calculations, however, indicated five degenerate transitions present in the B-band region of the UV−vis and MCD spectra of PcZn, while the presence of such transitions was not confirmed experimentally in band deconvolution analysis.[10,14,16] Mack et al., however, in a very recent review indicated that TDDFT-predicted vertical excitation energies for transition-metal phthalocyanines should be used with great caution, again because their deconvolution
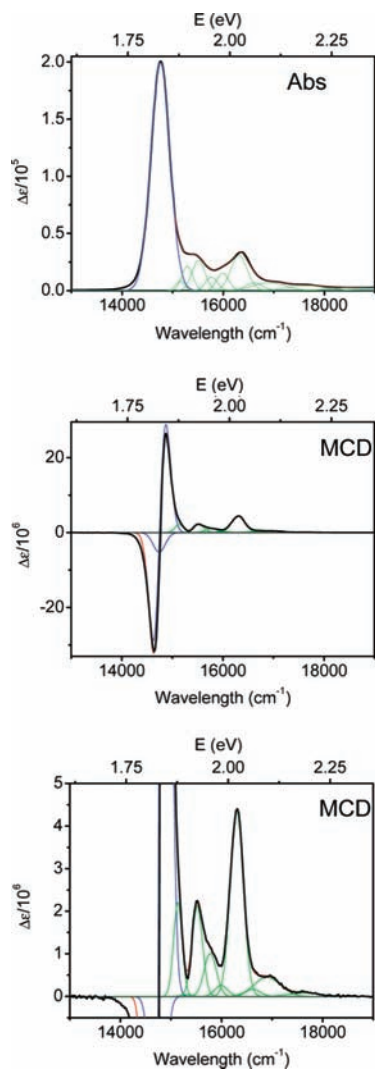
Figure 15. Band deconvolution analysis of UV−vis and MCD spectra of Pc^{t}Zn in the Q-band region: experimental data, black line; cumulative fit curve, red line; MCD *A*-term, blue lines; MCD *B*-term, green lines.

TABLE 3: Band Deconvolution Analysis Parameters for Pc^{t}Zn in Dichloromethane

band number	E (eV)	λ (nm)	Δ^a (eV)	Faraday MCD term
1	1.83	678	0.0280	*A*
2	1.90	653	0.0133	*B*
3	1.88	661	0.0105	*B*
4	1.92	644	0.0129	*B*
5	1.96	634	0.0150	*B*
6	1.98	625	0.0155	*B*
7	2.02	613	0.0161	*B*
8	2.06	602	0.0176	*B*
9	2.10	592	0.0322	*B*
10	2.19	566	0.0399	*B*
11	2.32	534	0.0614	*B*
12	3.02	410	0.0725	*A*
13	3.15	393	0.107	*A*
14	3.23	384	0.124	*B*
15	3.34	371	0.0748	*A*
16	3.50	354	0.127	*A*
17	3.61	344	0.202	*A*
18	3.83	324	0.172	*A*
19	4.15	298	0.112	*B*
20	4.36	284	0.0984	*A*^{b}

^{a} Band half-width. ^{b} Part of the L-band spectral envelope

models are in disagreement with the TDDFT calculations.[25] To date, the majority of simultaneous band deconvolution analyses of MCD and UV−vis spectra of PcZn and other divalent main group transition metals belong to Stillman's group, which uses the home-made SIMPFIT program for data analysis.[49] Interestingly, the spectra deconvolution model for the B-band region also evolves from this research group. Indeed, for the B-band region, early UV−vis and MCD data for axially ligated PcZn and PcMg complexes were fit using two degenerate and several nondegenerate transitions.[10,50] Later, the same group provided a low-temperature analysis of UV−vis and MCD spectra of an axially ligated PcZn complex and suggested the presence of five nondegenerate transitions in the same spectral region.[14] Finally, recently, the same group used again two degenerate and a number of nondegenerate transitions in the UV−vis and MCD band deconvolution analysis of fluorinated zinc phthalocyanines.[16] The question remaining open is whether or not it is possible to receive a good fit of experimental data pertaining to PcZn using TDDFT-predicted vertical excitation energies while taking into consideration the amount of error that is typical for TDDFT calculations. To address this question, we conducted band deconvolution analyses of room-temperature UV−vis and MCD spectra of the Pc^{t}Zn complex considering vertical excitation energies predicted using BP86 and B3LYP exchange-correlation functionals in tandem with a molecular geometry

optimized at the B3LYP level. We chose the Pc^{t}Zn complex to gain experimental data because: (i) use of axially ligated PcZnL complexes leads to a deviation of the central atom from the N$_4$ plane and results in a lowering of effective symmetry of these complexes from D_{4h} to C_{4v}, while the influence of the *tert*-butyl substituents on the effective symmetry in Pc^{t}Zn is negligibly small, and thus, this complex retains D_{4h} symmetry with the central atom being four-coordinated; (ii) axial coordination of nitrogen bases or cyanide ion to PcZn, as was the case for Stillman's group, significantly affects the energies of electronic transitions observed in the B-band spectral envelope. Indeed, the B-band spectral envelope observed in the case of argon-isolated PcZn and in the case of a room-temperature solution of Pc^{t}Zn is located between 2.85 and 4.09 eV,[12] while that observed in PcZnL complexes was observed between 2.60 and 4.22 eV.[10,14] More importantly, in the case of tetracoordinated PcZn[12] and Pc^{t}Zn complexes, the B-band region consists of a single negative component of a MCD Faraday *A*-term, while two negative components of MCD Faraday *A*-terms were observed in the case of PcZnL complexes.[10,14,16] (iii) Pc^{t}Zn is very soluble in a variety of non-coordinating solvents that are transparent in a wide spectral range.
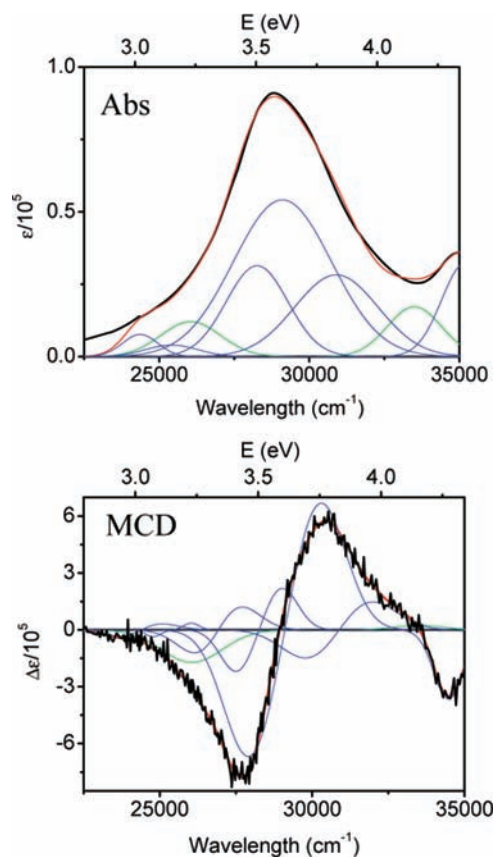
Q-Band Region. Band deconvolution analysis of the UV−vis and MCD spectra of Pc^{t}Zn in the Q-band spectral envelope is presented in Figure 15 and Table 3. The MCD spectrum was deconvoluted using a single prominent Faraday *A*-term followed by a series of positive Faraday *B*-terms with lower intensities. In agreement with the previous assignments[6,8,10,12,14] and in accord with our TDDFT and PCM-TDDFT calculations, the strong Q-band observed at 1.83 eV in the UV−vis spectrum and the Faraday *A*-term centered at 1.83 eV in the MCD spectrum of Pc^{t}Zn can be clearly attributed to the 1^{1}E$_u$ excited state. The lower-intensity, higher-energy bands observed in the Q$_{0-1}$ and Q$_{0-2}$ band regions of Pc^{t}Zn can be easily attributed to vibronic progressions originating from the Q$_{0-0}$ electronic transition.[6] Taking into consideration the experimental temperature for acquisition of UV−vis and MCD spectra of Pc^{t}Zn, it is hard to expect that additional information on such vibronic transitions will be useful in future analyses.

The analysis of Huang et al. of Spol'ski matrix data[51] as well as a more recent UV−vis and MCD band deconvolution analysis

TDDFT and PCM-TDDFT in Phthalocyanines

J. Phys. Chem. A, Vol. 111, No. 50, 2007 **12911**

TABLE 4: Gas-Phase TDDFT-Predicted Vertical Excitation Energies in PcZn Using Pure BP86 Exchange-Correlation Functional and Centers of Experimentally Observed Bands from Band Deconvolution Analysis

transition	BP86 E (eV)	experimental E (eV)
$1\ ^1E_u$	2.00	1.83
$1\ ^1E_g$	2.15	2.02
$2\ ^1E_u$	2.88	3.02
$3\ ^1E_u$	3.09	3.15
$4\ ^1E_u$	3.15	3.34
$1\ ^1A_{2u}$	3.16	3.23
$5\ ^1E_u$	3.45	3.50
$6\ ^1E_u$	3.50	3.61
$2\ ^1A_{2u}$	3.80	4.15
$7\ ^1E_u$	3.82	3.83

of argon matrix data by VanCott et al.[12] for PcZn suggested the presence of an additional n → π* electronic transition in the Q_{0-2} region at ca 2.05 eV. This transition was assigned to a $19e_u$ (N_{meso} lone pair) → $7e_g$ (LUMO) excitation by VanCott et al.[12] as well as Mack and Stillman.[17] The presence of the lowest z-polarized 1^1A_{2u} state in the Q_{0-2} region, however, has never been confirmed computationally at either semiempirical or TDDFT levels of theory. As mentioned above, the relative energies of the predominantly nitrogen lone-pair-based molecular orbitals are extremely sensitive to the theoretical method and exchange-correlation functional (in the case of TDDFT calculations) used in the calculations. In all DFT calculations, the nitrogen-based $19e_u$ molecular orbitals have energies well below the HOMO and are within the energies of the occupied π-orbitals that are involved in the formation of the B-band region of the UV−vis and MCD spectra of PcZn. Not surprisingly, the first TDDFT-calculated electronically allowed 1^1A_{2u} state was observed in the B-band region rather than the Q_{0-2} spectral envelope. We would like to point out, however, that the HOMO − 1 molecular orbital calculated using a DFT approach coupled with pure exchange-correlation functionals is $11b_{1g}$, which predominantly consists of pyrrolic nitrogen lone pairs. Accordingly, an electronic transition from this orbital to the LUMO ($11b_{1g}$ → $7e_g$) results in the 1^1E_g excited state with a predicted energy close to that suggested by Huang et al. and VanCott et al. for the position of the first n → π* band in the Q_{0-2} band spectral envelope (Supporting Information Table 4). Although the $11b_{1g}$ → $7e_g$ transition is electronically forbidden, coupling of the 1^1E_g excited state with an e_u symmetry fundamental skeletal vibrational normal mode of the phthalocyanine core can easily result in a weak z-polarized absorption band located in the Q_{0-2} region, observed even at low temperatures. Taking into account that TDDFT calculations with pure exchange-correlation functionals give a closer (in comparison to the hybrid ones) agreement between theory and experiment, we would like to suggest that the band observed in the Q_{0-2} spectral envelope is a vibronically allowed $11b_{1g}$ → $7e_g$ transition. Such an assignment can, indeed, resolve the long-time disagreement between experimental evidence of the presence of a z-polarized band in the Q_{0-2} band region and previous theoretical predictions. Because it is difficult to prove experimentally to which of the vibration modes the z-polarized absorption band located in the Q_{0-2} region belongs to, it will be interesting to confirm our assumption using more accurate quantum mechanical calculations in the future. So far, all CASPT2,[52] SAC-CI,[53] and DFT/MRCI[54] results published on phthalocyanine systems involved calculations regarding only π−π* transitions, while the high computational cost of these methods along with the limited computational resources did not allow us to obtain additional insight into the energies of n−π* transitions of interest.

Figure 16. Band deconvolution analysis of UV−vis and MCD spectra of Pc′Zn in the B-band region: experimental data, black line; cumulative fit curve, red line; MCD *A*-term, blue lines; MCD *B*-term, green lines.

B-Band Region. Band deconvolution analysis of UV−vis and MCD spectra of Pc′Zn in the B-band spectral envelope is presented in Figure 16 and Table 3. As mentioned above, UV−vis and MCD spectra of Pc′Zn are very close to those obtained for PcZn in an argon matrix[12] but differ significantly from those of pentacoordinated PcZnL complexes described by Stillman's group.[10,14] It should be noted that the number and the nature of excited states contributing to the B-band spectral envelope remains unclear despite the large experimental effort provided by several research groups. In the majority of band deconvolution analyses conducted by Stillman's group on PcZnL complexes,[10,16,17] two Faraday *A*-terms were used in the B-band spectral envelope, while VanCott et al.[12] suggested the presence of at least three electronic transitions in this region. Moreover, low-temperature argon matrix experiments clearly indicate the presence of vibrational progression for the lowest energy band observed in the B-band region, and such progression has never been taken into consideration by Stillman's group in band deconvolution analyses. Finally, the low-temperature band deconvolution analysis of the [PcZnCN]⁻ complex provided recently by Stillman's group[14] resulted in five bands originating from two Jahn−Teller splitted Faraday *A*-terms and a single *B*-term, but this strategy was criticized later by Ricciardi et al.[15] Indeed, it is hard to believe that the Q_{0-0} electronic transition does not exhibit a small Jahn−Teller distortion, while similar π → π* electronic transitions responsible for the observed ^1E_u excited states in the B-band region do exhibit large (on the order of 0.124 eV) Jahn−Teller distortions. Overall, reasonably assuming the presence of vibronic bands for each allowed electronic transition, the band deconvolution analysis of the B-band spectral envelope is a very challenging task. This task can be accomplished, however, if accurate methods for the

prediction of vertical excitation energies in phthalocyanines and related compounds can be found. Taking into consideration that the TDDFT approach coupled with pure exchange-correlation functionals gives very good agreement between theory and experiment in the Q-band region, we tried to conduct band deconvolution analyses of the B-band spectral envelope using TDDFT-predicted vertical excitation energies as a starting approximation. TDDFT calculations using a BP86 exchange-correlation functional and a molecular geometry optimized using the B3LYP method predict six degenerate ^1E_u excited states and two nondegenerate $^1A_{2u}$ excited states in the B-band region. In the first attempt of a simultaneous band deconvolution analysis, we have ignored all possible vibronic satellites of electronically allowed transitions as well as the possible vibronically allowed z-polarized band arising from the coupling of the 2^1E_g excited state with an e_u vibration of the phthalocyanine core. Accordingly, the B-band spectral envelope was deconvoluted using only six degenerate and two nondegenerate transitions. In spite of the oversimplified model used for the band deconvolution analysis, the agreement between vertical excitation energies obtained theoretically and experimentally is excellent (Table 4), suggesting that modern TDDFT methods, indeed, can be used for the accurate prediction of absorption spectra in complex macrocyclic systems. Of course, our initial model can only serve as a proof of the concept. Indeed, addition of the vibronic components to the allowed electronic transitions observed in the B-band spectral envelope as well as considering the presence of the 2^1E_g excited state in the low-energy limit of B-band region will further improve the quality of band deconvolution analyses in Pc'Zn. The positions of these vibronic satellites, however, are not clear and currently cannot be resolved by spectroscopic methods, making an accurate experiment-based band deconvolution analysis in the B-band region virtually impossible. Of course, experimentally, it is hard to prove the presence of eight electronic transitions in the B-band region because of the severe overlap between these electronic transitions and the presence of their vibronic components in this spectral envelope. Such a severe overlap cannot be resolved even in matrix-isolated samples in the low-temperature limit. On the other hand, and consistent with the closely spaced π-orbitals calculated at the DFT level, an excellent agreement observed between calculated vertical excitation energies and band energies used in the band deconvolution analyses allows us to suggest the presence of numerous electronic transitions in the B-band spectral envelope.

Conclusions

A TDDFT approach coupled with 14 different exchange-correlation functionals was used for the prediction of vertical excitation energies of zinc phthalocyanine (PcZn). In general, the TDDFT approach provides a more accurate description of both visible and ultraviolet regions of UV−vis spectra of PcZn in comparison to the more popular semiempirical ZINDO/S and PM3 methods. It was found that the calculated vertical excitation energies of PcZn correlate with the amount of Hartree−Fock exchange involved in the exchange-correlation functional. This correlation was explained on the basis of the calculated difference in energy between occupied and unoccupied molecular orbitals. The influence of PcZn geometry, optimized using different exchange-correlation functionals, on the calculated vertical excitation energies in PcZn was found to be relatively small. The influence of solvents on the calculated vertical excitation energies in PcZn was considered for the first time using a PCM-TDDFT method and was found to be small, in an

excellent agreement with the experimental data. For all tested TDDFT and PCM-TDDFT cases, an assignment of the Q-band as an almost pure $2a_{1u}$ (HOMO) → $7e_g$ (LUMO) transition, initially suggested by Gouterman, was confirmed. Pure exchange-correlation functionals indicate the presence of six ^1E_u states in the B-band region of the UV−vis spectrum of PcZn, while hybrid exchange-correlation functionals predict only five ^1E_u states for the same energy envelope. The first two symmetry-forbidden n → π* transitions were predicted in the Q_{0-2} band region, while the symmetry-allowed n → π* transitions were found within the B-band energy envelope when pure DFT exchange-correlation functionals were used in TDDFT calculations. The presence of a symmetry-forbidden but vibronically allowed n → π* transition in the Q_{0-2} spectral envelope explains the long-time controversy between the experimentally observed low-intensity transition in the Q_{0-2} region and previous semiempirical and TDDFT calculations, which were unable to predict any electronic transitions in this area. To prove the conceptual possibility of the presence of several degenerate ^1E_u states in the B-band region of PcZn, room-temperature UV−vis and MCD spectra of Pc'Zn in non-coordinating solvents were recorded and analyzed using band deconvolution analysis. It was found that the B-band region of the UV−vis and MCD spectra of Pc'Zn can be easily deconvoluted using several MCD A-terms with energies close to those predicted by TDDFT calculations for ^1E_u excited states. Such a good agreement between theory and experiment clearly indicates the possibility of employing a TDDFT approach for the accurate prediction of vertical excitation energies in phthalocyanines within a large energy range.

References and Notes

(1) *Phthalocyanines: Properties and Applications*; Leznoff, C. C., Lever, A. B. P., Eds.; VCH Publishers: New York, 1990−1996; Vol. 1−4.

(2) McKeown, N. B.; Budd, P. M. *Chem. Soc. Rev.* **2006**, *35*, 675−683. Kaliya, O. L.; Lukyanets, E. A.; Vorozhtsov, G. N. *J. Porphyrins Phthalocyanines* **1999**, *3*, 592−610.

(3) (a) Juzenas, P. *Trends Cancer Res.* **2005**, *1*, 93−110. (b) O'Riordan, K.; Akilov, O. E.; Hasan, T. *Photodiagn. Photodyn. Ther.* **2005**, *2*, 247−262.

(4) (a) Elemans, J. A. A. W.; van Hameren, R.; Nolte, R. J. M.; Rowan, A. E. *Adv. Mater.* **2006**, *18*, 1251−1266. (b) Rao, C. N. R.; Govindaraj, A. *Acc. Chem. Res.* **2002**, *35*, 998−1007.

(5) (a) de la Torre, G.; Vazquez, P.; Agullo-Lopez, F.; Torres, T. *J. Mater. Chem.* **1998**, *8*, 1671−1683. (b) Chen, Y.; Hanack, M.; Blau, W. J.; Dini, D.; Liu, Y.; Lin, Y.; Bai, J. *J. Mater. Sci.* **2006**, *41*, 2169−2185. (c) Wrobel, D.; Dudkowiak, A. *Mol. Cryst. Liq. Cryst.* **2006**, *448*, 617−640.

(6) Stillman, M. J. In *Phthalocyanines: Properties and Applications*; Leznoff, C. C., Lever, A. B. P., Eds.; VCH Publishers: New York, 1993; Vol. 3, Chapter 5, pp 227−296.

(7) Anderson, J. S.; Bradbrook, E. F.; Cook, A. H.; Linstead, R. P. *J. Chem. Soc.* **1938**, 1151−1156.

(8) Edwards, L.; Gouterman, M. *J. Mol. Spectrosc.* **1970**, *33*, 292.

(9) Edwards, L.; Dolphin, D. H.; Gouterman, M. *J. Mol. Spectrosc.* **1970**, *35*, 90.

(10) Nyokong, T. N.; Gasyna, Z.; Stillman, M. J. *Inorg. Chem.* **1987**, *26*, 1087.

(11) Mack, J.; Stillman, M. J. *J. Phys. Chem.* **1995**, *99*, 7935.

(12) VanCott, T. C.; Rose, J. L.; Misener, G. C.; Williamson, B. E.; Schrimpf, A. E.; Boyle, M. E.; Schatz, P. N. *J. Phys. Chem.* **1989**, *93*, 2999.

(13) Fitch, P. S. H.; Wharton, L.; Levy, D. H. *J. Chem. Phys.* **1978**, *69*, 3424−3426.

(14) Mack, J.; Stillman, M. J. *J. Phys. Chem.* **1995**, *99*, 7935.

(15) Ricciardi, G.; Rosa, A.; Baerends, E. J. *J. Phys. Chem. A* **2001**, *105*, 5242−5254.

(16) Keizer, S. P.; Mack, J.; Bench, B. A.; Gorun, S. M.; Stillman, M. J. *J. Am. Chem. Soc.* **2003**, *125*, 7067−7085.

(17) Mack, J.; Stillman, M. J. *Coord. Chem. Rev.* **2001**, *219−221*, 993−1032.

(18) (a) Deeth, R. J. *Faraday Discuss.* **2003**, *124*, 379−391. (b) Rosa, A.; Ricciardi, G.; Gritsenko, O.; Baerends, E. J. *Struct. Bonding* **2004**, *112*, 49−116. (c) Nemykin, V. N.; Basu, P. *Inorg. Chem.* **2003**, *42*, 4046−4056.

(19) (a) Roitberg, A. E.; Worthington, S. E.; Holden, M. J.; Mayhew, M. P.; Krauss, M. *J. Am. Chem. Soc.* **2000**, *122*, 7312−7316. (b) Schlegel, H. B.; Robb, M. A. *Chem. Phys. Lett.* **1982**, *93*, 43−46.

(20) (a) Shepard, R.; Shavitt, I.; Pitzer, R. M.; Comeau, D. C.; Pepper, M.; Lischka, H.; Szalay, P. G.; Ahlrichs, R.; Brown, F. B.; Zhao, J.-G. *Int. J. Quantum Chem.* **1988**, *S2*, 149−165. (b) Lischka, H.; Dallos, M.; Shepard, R. *Mol. Phys.* **2002**, *100*, 1647−1658. (c) Chang, J.-L.; Chen, Y.-T. *J. Chem. Phys.* **2002**, *116*, 7518−7525.

(21) (a) Hesselmann, A.; Jansen, G.; Schuetz, M. *J. Am. Chem. Soc.* **2006**, *128*, 11730−11731. (b) Podeszwa, R.; Bukowski, R.; Szalewicz, K. *J. Chem. Theory Comput.* **2006**, *2*, 400−412.

(22) Dreuw, A.; Head-Gordon, M. *Chem. Rev.* **2005**, *105*, 4009−4037.

(23) Nguyen, K. A.; Pachter, R. *J. Chem. Phys.* **2001**, *114*, 10757−10767.

(24) Mack, J.; Asano, Y.; Kobayashi, N.; Stillman, M. J. *J. Am. Chem. Soc.* **2005**, *127*, 17697−17711.

(25) Mack, J.; Stillman, M. J.; Kobayashi, N. *Coord. Chem. Rev.* **2007**, *251*, 429−453.

(26) Kuznetsova, N. A.; Okunchikov, V. V.; Derkacheva, V. M.; Kaliya, O. L.; Lukyanets, E. A. *J. Porphyrins Phthalocyanines* **2005**, *9*, 393−397.

(27) Becke, A. D. *Phys. Rev. A* **1988**, *38*, 3098−3100.

(28) Perdew, J. P. *Phys. Rev. B* **1986**, *33*, 8822−8824.

(29) Becke, A. D. *J. Chem. Phys.* **1993**, *98*, 5648−5652.

(30) Lee, C.; Yang, W.; Parr, R. G. *Phys. Rev. B* **1988**, *37*, 785−789.

(31) Perdew, J. P.; Burke, K.; Ernzerhof, M. *Phys. Rev. Lett.* **1996**, *77*, 3865.

(32) (a) McLean, A. D.; Chandler, G. S. *J. Chem. Phys.* **1980**, *72*, 5639−5948. (b) Krishnan, R.; Binkley, J. S.; Seeger, R.; Pople, J. A. *J. Chem. Phys.* **1980**, *72*, 650−654.

(33) (a) Miertus, S.; Scrocco, E.; Tomasi, J. *Chem. Phys.* **1981**, *55*, 117−129. (b) Tomasi, J.; Mennucci, B.; Cammi, R. *Chem. Rev.* **2005**, *105*, 2999−3094.

(34) (a) Ridley, J.; Zerner, M. C. *Theor. Chim. Acta* **1973**, *32*, 111−134. (b) Zerner, M. C.; Loew, J. H.; Kirchner, E. F.; Mueller-Westerhoff, U. T.; Nazaal, A. *J. Am. Chem. Soc.* **1980**, *102*, 589−599. (c) Neto, J. D.

M.; Zerner, M. C. *Int. J. Quantum Chem.* **2001**, *81*, 187−201. (d) Anderson, W. P.; Edwards, E. D.; Zerner, M. C. *Inorg. Chem.* **1986**, *25*, 2728−2732.

(35) Stewart, J. J. P. *J. Comput.-Aided Mol. Des.* **1990**, *4*, 1−105.

(36) Frisch, M. J.; Trucks, G. W.; Schlegel, H. B.; Scuseria, G. E.; Robb, M. A.; Cheeseman, J. R.; Montgomery, J. A. Jr.; Vreven, T.; Kudin, K. N.; Burant, J. C.; Millam, J. M.; Iyengar, S. S.; Tomasi, J.; Barone, V.; Mennucci, B.; Cossi, M.; Scalmani, G.; Rega, N.; Petersson, G. A.; Nakatsuji, H.; Hada, M.; Ehara, M.; Toyota, K.; Fukuda, R.; Hasegawa, J.; Ishida, M.; Nakajima, T.; Honda, Y.; Kitao, O.; Nakai, H.; Klene, M.; Li, X.; Knox, J. E.; Hratchian, H. P.; Cross, J. B.; Bakken, V.; Adamo, C.; Jaramillo, J.; Gomperts, R.; Stratmann, R. E.; Yazyev, O.; Austin, A. J.; Cammi, R.; Pomelli, C.; Ochterski, J. W.; Ayala, P. Y.; Morokuma, K.; Voth, G. A.; Salvador, P.; Dannenberg, J. J.; Zakrzewski, V. G.; Dapprich, S.; Daniels, A. D.; Strain, M. C.; Farkas, O.; Malick, D. K.; Rabuck, A. D.; Raghavachari, K.; Foresman, J. B.; Ortiz, J. V.; Cui, Q.; Baboul, A. G.; Clifford, S.; Cioslowski, J.; Stefanov, B. B.; Liu, G.; Liashenko, A.; Piskorz, P.; Komaromi, I.; Martin, R. L.; Fox, D. J.; Keith, T.; Al-Laham, M. A.; Peng, C. Y.; Nanayakkara, A.; Challacombe, M.; Gill, P. M. W.; Johnson, B.; Chen, W.; Wong, M. W.; Gonzalez, C.; Pople, J. A. *Gaussian 03*, revision C.02; Gaussian, Inc.: Wallingford, CT, 2004.

(37) *HyperChem Pro*, version 7.51; HyperCube, Inc.: Gainesville, FL, 2004.

(38) Nemykin, V. N.; Basu, P. VMOdes: Virtual Molecular Orbital description program for Gaussian, GAMESS, and HyperChem, revision A 7.1, 2004.

(39) *Origin Pro*, version 7.5; OriginLab Corporation: Northampton, MA, 2004.

(40) Scheid, W. R.; Dow, W. *J. Am. Chem. Soc.* **1977**, *99*, 1101.

(41) (a) Wu, Q.; Cohen, A. J.; Yang, W. *J. Chem. Phys.* **2005**, *123*, 134111. (b) Dierksen, M.; Grimme, S. *J. Phys. Chem. A* **2004**, *108*, 10225−10237. (c) Leszcynski, J.; Goodman, L.; Kwiatkowski, J. S. *Theor. Chem. Acc.* 1997, *97*, 195−202. (d) Lelj, F.; Adamo, C.; Barone, V. *Chem. Phys. Lett.* **1994**, *230*, 189−95.

(42) Nemykin, V. N.; Hadt, R. G. *Inorg. Chem.* **2006**, *45*, 8297−8307.

(43) Schlettwein, D.; Hesse, K.; Gruhn, N. E.; Lee, P. A.; Nebesny, K. W.; Armstrong, N. R. *J. Phys. Chem. B* **2001**, *105*, 4791−4800.

(44) Van, Voorhis, T.; Scuseria, G. E. *J. Chem. Phys.* **1998**, *109*, 400.

(45) Martin, C. H.; Zerner, M. C. In *Inorganic Electronic Structure and Spectroscopy*; Solomon, E. I., Lever A. B. P., Eds.; Wiley: New York, 1999; Vol. 1, pp 555−659.

(46) (a) Wan, J.; Ren, Y.; Wu, J.; Xu, X. *J. Phys. Chem. A* **2004**, *108*, 9453−9460. (b) Chakraborty, A.; Kar, S.; Nath, D. N.; Guchhait, N. *J. Phys. Chem. A* **2006**, *110*, 12089−12095. (c) Zhu, Y.; Zhou, S.; Kan, Y.; Su, Z. *Int. J. Quantum Chem.* **2007**, *107*, 1614−1623. (d) Nemykin, V. N.; Olsen, J. G.; Perera, E.; Basu, P. *Inorg. Chem.* **2006**, *45*, 3557−3568.

(47) (a) *HyperChem Reference Manual*; HyperCube, Inc.: Gainesville, FL, 1996. (b) Parr, R. G. *The Quantum Chemistry of Molecular Electronic Structure*; W. A. Benjamin: New York, 1964; p 510.

(48) Yuan, S.; Feng Chen, Z.; Rong. *J. Phys. Chem. A* **2005**, *109*, 2582−2585.

(49) Browett, W. R.; Stillman, M. *J. Comput. Chem.* **1987**, *11*, 241.

(50) Ough, E.; Nyokong, T.; Creber, K. A. M.; Stillman, M. J. *Inorg. Chem.* **1988**, *27*, 2724−2732.

(51) Huang, T. H.; Reickhoff, K. E.; Voigt, E. M. *J. Chem. Phys.* **1982**, *77*, 3424−3441.

(52) Scheidt, W. R.; Dow, W. *J. Am. Chem. Soc.* **1977**, *36*, 413.

(53) Cortina, H.; Senent, M. L.; Smeyers, Y. G. *J. Phys. Chem. A* **2003**, *107*, 8968.

(54) Toyota, K.; Hasegawa, J.; Nakatsuji, H. *J. Phys. Chem. A* **1997**, *101*, 446.

(55) Parusel, A. B. J.; Grimme, S. *J. Porphyrins Phthalocyanines* **2001**, *5*, 225.